Published in final edited form as:
Neuroimage. 2011 May 1; 56(1): 268–279. doi:10.1016/j.neuroimage.2010.09.040.

Evaluation of [^{11}C]MRB for assessment of occupancy of norepinephrine transporters: Studies with atomoxetine in non-human primates

Jean-Dominique Gallezot[a,*], **David Weinzimmer**[a], **Nabeel Nabulsi**[a], **Shu-Fei Lin**[a], **Krista Fowles**[a], **Christine Sandiego**[a], **Timothy J. McCarthy**[b], **R. Paul Maguire**[b], **Richard E. Carson**[a], and **Yu-Shin Ding**[a]

[a]PET Center, Department of Diagnostic Radiology, Yale University, New Haven, CT 06520, USA

[b]Pfizer Global R&D, Groton, CT 06340, USA

Abstract

[^{11}C]MRB is one of the most promising radioligands used to measure brain norepinephrine transporters (NET) with positron emission tomography (PET). The objective of this study was to evaluate the suitability of [^{11}C]MRB for drug occupancy studies of NET using atomoxetine (ATX), a NET uptake inhibitor used in the treatment of depression and attention-deficit hyperactivity disorder (ADHD). A second goal of the study was identification of a suitable reference region. Ten PET studies were performed in three anesthetized rhesus monkeys following an infusion of ATX or placebo. [^{11}C]MRB arterial input functions and ATX plasma levels were also measured. A dose-dependent reduction of [^{11}C]MRB volume of distribution was observed after correction for [^{11}C]MRB plasma free fraction. ATX IC_{50} was estimated to be 31±10 ng/mL plasma. This corresponds to an effective dose (ED_{50}) of 0.13 mg/kg, which is much lower than the therapeutic dose of ATX in ADHD (1.0–1.5 mg/kg). [^{11}C]MRB binding potential BP_{ND} in the thalamus was estimated to be 1.8±0.3. Defining a reference region for a NET radiotracer is challenging due to the widespread and relatively uniform distribution of NET in the brain. Three regions were evaluated for use as reference region: caudate, putamen and occipital cortex. Caudate was found to be the most suitable for preclinical drug occupancy studies in rhesus monkeys. The IC_{50} estimate obtained using MRTM2 BP_{ND} without arterial blood sampling was 21±3 ng/mL (using caudate as the reference region). This study demonstrated that [^{11}C]MRB is suitable for drug occupancy studies of NET.

Introduction

The brain norepinephrine transporter (NET) is responsible for norepinephrine reuptake, as well as dopamine reuptake in some regions such as the frontal cortex. (Morón et al., 2002). The ability to quantify the density of these transporters *in vivo* with positron emission tomography (PET) would provide an important means to study the role of NET in various psychiatric and behavioral disorders in which they are implicated, such as attention deficit hyperactivity disorder (ADHD) (Spencer et al., 2002), substance abuse and depression (Barker and Blakely, 1995; Ding et al., 2006, review and references within). However, PET imaging of norepinephrine transporters has long been hampered by the lack of suitable radioligand (Ding et al., 2005, 2006). Drawbacks of early candidate radiotracers included

*Corresponding author. PET Center, Yale School of Medicine, P.O. Box 208048, New Haven, CT 06520-8048, USA. Fax: +1 203 785 3107. jean-dominique.gallezot@yale.edu. .

very low specific binding and the lack of a suitable reference region. The challenges for NET imaging are in part fundamentally due to the widespread distribution of NET in the brain, and the lower contrast in transporter density between NET-poor and NET-rich regions (Smith et al., 2006) than for the other monoamine transporters like DAT (Kaufman et al., 1991) or SERT (Zeng et al., 2006). Furthermore, the locus coeruleus, the highest NET density region, is difficult to localize and quantify with PET due to its small volume. Currently, the best radioligands available are derivatives of reboxetine: (S,S)-[^{11}C]methylreboxetine ([^{11}C]MRB, also known as [^{11}C]MeNER) (Ding et al., 2003; Schou et al., 2003; Wilson et al., 2003) and its [^{18}F]fluoromethyl derivatives ([^{18}F]F-MeNER-D$_2$ (Schou et al., 2004) and [^{18}F]FRB (Ding et al., 2005, Lin et al., 2005). They have higher specific binding and lower variability in non-specific binding than previous radioligands (Ding et al., 2006).

When [^{11}C]MRB was initially tested in a drug occupancy study in humans using Atomoxetine (ATX), a reduction in [^{11}C]MRB binding was reported, but there was no obvious dose-dependent effect (Logan et al., 2007). ATX is a potent norepinephrine transporter reuptake inhibitor (K_i ~ 5 nM) currently used in the treatment of depression and ADHD (Spencer et al., 2002). One hypothesis was that the doses of ATX examined in the human PET study, though clinically relevant, were too high. That is, the three tested doses all reached saturation, the plateau portion of the corresponding dose-occupancy curve, and, as a result, there was no obvious dose-dependent effect. Another occupancy study of ATX using [^{18}F]F-MeNER-D$_2$ in rhesus monkeys showed a reasonable dose-dependent occupancy though only in one of the two monkeys studied and the IC_{50} (or ED_{50}) was not determined (Seneca et al., 2006). In a second occupancy study of ATX using [^{18}F]F-MeNER-D$_2$ in rhesus monkeys, the ATX IC_{50} was quantified as 16 ng/mL plasma (Takano et al., 2009a), which is about 7 times lower than the lowest plasma levels achieved in the aforementioned [^{11}C]MRB human study.

The goal of the study was to re-evaluate the suitability of [^{11}C]MRB for occupancy studies in non-human primates using lower doses of ATX than those used in the previous PET study with [^{11}C]MRB (Logan et al., 2007), and with a continuous ATX infusion paradigm, a protocol similar to the aforementioned [^{18}F]F-MeNER-D$_2$ studies. A second goal of this study is to determine if there is a suitable reference region for [^{11}C]MRB.

Materials and methods

Study design

In order to maintain a constant concentration of ATX in the plasma during the PET acquisition time, a continuous infusion protocol was used. This protocol was similar to the one used in the study with [^{18}F]F-MeNER-D$_2$ (Seneca et al., 2006). Two infusion rates were used (Fig. 1): 2 h before the beginning of each PET scan, the first ATX infusion at the "loading" rate was begun; then, 1 h before the injection of [^{11}C]MRB and the beginning of the PET scan, the infusion rate was lowered by 37.5% (i.e., "maintenance" rate). This infusion rate (MIR_{ATX}) was maintained until the end of PET scan. Initially the maintenance rates were 0.01 mg/kg/h (low dose), 0.05 mg/kg/h (medium dose) and 0.012 mg/kg/h (high dose). After analysis of the data from the first two monkeys (6 scans), the medium and high-dose rates were lowered to 0.03 mg/kg/h and 0.09 mg/kg/h, respectively.

The design was to have each monkey have four PET scans on 2 study days. These 2 study days were scheduled 2 weeks apart to allow recovery from the effects of the anesthesia and blood drawing. On each study day, two PET scans were acquired, beginning 4 h apart. The first study day consisted of the baseline and medium-dose scans, the second study day consisted of the low- and high-dose scans.

Study population

Three non-human primates (Rhesus macaque, 5.5±1.4 years old and weighing 6.7±1.4 kg) were scanned. Only two monkeys were scanned four times. The second monkey could not be scanned on the second study day, due to the unavailability of arterial samples. Thus, only baseline and medium-dose scans were acquired for that animal. All study procedures were performed under a protocol approved by the Yale University Institutional Animal Care and Use Committee.

Radiochemistry

Both the MRB standard and precursor were prepared previously (Lin and Ding, 2004). [^{11}C]MRB was synthesized with [^{11}C]methyliodide ([^{11}C]MeI) as previously reported (Lin and Ding, 2004) except, radiolabeling was carried out using either the TRACERLab FXC automated synthesis module (GE Medical Systems), or using the AutoLoop (Bioscan, Washington, DC, USA) by modifying previously reported method (Wilson et al., 2003) (see supplementary information for details). C-11 methyl iodide ([^{11}C]CH_3I) was produced from [^{11}C] CO_2, as previously described (Nabulsi et al., 2010). The total radio-synthesis time was ~40 min with an average specific activity of 264±107 MBq/nmol (7±3 mCi/nmol) at the end of synthesis (n=10). The final formulated product was >98% radiochemically pure. The average injected dose was 247±20 MBq with an average specific radioactivity of 129±46 MBq/nmol at the time of injection. The average injected mass was 0.57±0.23 μg.

PET imaging

Animals were initially anesthetized with an intramuscular injection of ketamine hydrochloride, intubated and transported to the PET facility. They were maintained on oxygen and isoflurane (1.5–3%) throughout the study. Scans were performed with the High Resolution Research Tomograph (HRRT) (Siemens/CTI, Knoxville, TN, USA) PET scanner which acquires 207 simultaneous slices with 1.2 mm inter-slice distance and resolution of ~3 mm. Following a 6-min transmission scan, [^{11}C]MRB was injected over 2 min by an infusion pump (Harvard PHD 22/2000, Harvard Apparatus, Holliston, Massachusetts, United States). List-mode data were acquired for 120 min. Dynamic scan data were reconstructed with all corrections (attenuation, normalization, scatter, randoms, and deadtime) using the MOLAR algorithm (Carson et al., 2003; Johnson et al., 2004) with 2 iterations and 30 subsets. A sequence of 33 frames was reconstructed with the following timing: 6×30 s; 3×1 min; 2×2 min; 22×5 min.

Arterial input function measurement

In order to measure the time–concentration curve of [^{11}C]MRB, 21 blood samples were drawn at 0.5, 1, 1.5, 2, 2.5, 3, 4, 6, 8, 10, 15, 20, 25, 30, 40, 50, 60, 75, 90, 105, 120 min after the injection of [^{11}C]MRB. Sample volumes were approximately 0.5 mL. Samples drawn at 10-, 20-, 40-, 60- and 90-min postinjection had a volume of 1.5 mL in order to measure the fraction of unchanged [^{11}C]MRB in plasma by HPLC. Plasma was separated from blood cells by centrifugation (3900g for 5 min at 4 °C; Allegra X-22R Centrifuge, Beckman Coulter, Fullerton, CA, USA). Whole blood and plasma samples were counted in a cross-calibrated well counter (Wizard 1480, Perkin Elmer, Waltham, MA, USA).

For the metabolite samples, plasma proteins were precipitated using acetonitrile (1 mL/mL plasma) and centrifugation (14,000g for 5 min; Minispin plus centrifuge, Eppendorf, Westbury, NY, USA). The supernatant was counted and 0.2 mL was analyzed by reverse-phase HPLC. The HPLC system consisted of an isocratic pump (LC-20A1, Shimadzu, Kyoto, Japan), an injector (7725i, Rheodyne, Rohnert Park, CA, USA) equipped with a 2 mL sample loop, a Luna C18(2) column (semi-prep, 4.6×250 mm, 10 μm, Phenomenex,

Torrance, CA, USA). The column was eluted with a mixture of acetonitrile and aqueous 0.1 M ammonium formate (pH 4.2) in a ratio of 32:68 at a flow rate of ~4.2 mL/min. The output of the HPLC column was connected first to an UV detector (SPD-20A, Shimadzu, Kyoto, Japan), then to an inline gamma counter (Flow-Count Radio-HPLC Detector, Bioscan, Washington, DC, USA) and finally to a fraction collector (CF-1 Fraction Collector, Spectrum Chromatography, Houston, TX, USA). Collection tubes were manually shifted based on the detection of the parent compound peak with the inline gamma counter. Fractions were then counted in a well counter.

The ratios of the radioactivity concentrations in supernatant and plasma were obtained and fitted to a quadratic curve (f_S). The unchanged (i.e., unmetabolized) fraction of the tracer in the supernatant was fitted to an integrated gamma function:

$$f_H(t) = a \times \left(1 - b\int_0^{ct} e^{-u}u^{d-1}du \Big/ \int_0^{\infty} e^{-u}u^{d-1}du\right) \quad (1)$$

The unchanged tracer fraction in plasma was then computed as the product of the functions f_S and f_H. Both functions were extrapolated from 90 min (time of the last sample analyzed by HPLC) to 120 min.

[^{11}C]MRB plasma free fraction

For measurement of tracer plasma free fraction (f_p), ~740 kBq of [^{11}C] MRB was added (<25 μl/mL blood from the dose vial) to a blood sample withdrawn before injection to produce a blood standard. After mixing and centrifugation of red blood cells, plasma filtrate was separated from plasma proteins using ultrafiltration tubes (Centrifree UF device number 4104, Millipore, Billerica, MA, USA) and centrifugation (1100g for 20 min; IEC Medilite centrifuge, Thermo Fisher Scientific, Waltham, MA, USA). Plasma and filtrate samples were counted in triplicate and free fraction (f_P) was estimated as the ratio of the mean concentrations in filtrate and plasma.

ATX plasma levels

In addition to the samples used to determine [^{11}C]MRB radioactive concentration in plasma, four 3-mL blood samples were drawn 60, 120, 180, and 240 min post-ATX infusion (or 60 min before and 0, 60 and 120 min after tracer injection) to determine the ATX concentration in plasma. Red blood cells were precipitated; the plasma was frozen and then shipped for analysis. The plasma level of ATX was quantified with capillary gas chromatography-mass spectrometry (Analytical Psycho-pharmacology Laboratory, Nathan Kline Institute, Orangeburg, NY). The rate of variation of ATX concentration in plasma during the PET scan was estimated by fitting the 0-, 60- and 120-min sample values (post tracer injection) with a mono-exponential function.

Magnetic resonance imaging

MR images were acquired for each rhesus monkey on a Siemens 3.0T Trio scanner, using an extremity coil. T1-weighted images were acquired in the coronal plane with a spin echo sequence (TE=3.34, TR =2530, flip angle=7°, section thickness=0.50 mm, field-of-view = 140 mm, image matrix = 256 × 256 × 176 pixels, matrix size=0.5469×0.5469×0.5000 mm). Non-brain was removed and cropped to 176×176×176 pixels using MEDx software (Medical Numerics Inc, Germantown, MD, USA) before co-registration with PET Images.

Regional TAC computation

In order to compute regional time activity curves (TAC), selected regions of interest (ROIs) where drawn on a template brain (a representative MR image of a monkey brain, from a monkey not included in the study) for the caudate nucleus (0.43 cm^3), putamen (0.38 cm^3), occipital cortex (5.2 cm^3), anterior cingulate cortex (0.077 cm^3), thalamus (0.25 cm^3), midbrain (0.61 cm^3) and brainstem (1.85 cm^3). To transfer this template of regions to the PET dynamic images, two transformations were estimated: first, a nonlinear transform between the template MR image and each monkey MR image was computed using the bioimagesuite software (www.bioimagesuite.org); then, a rigid coregistration matrix was estimated between each monkey MR and an early PET sum image from each study (0–10 or 5–10 min postinjection), using a normalized mutual information algorithm (FLIRT, www.fmrib.ox.ac.uk/fsl/flirt/index.html).

Quantification of [^{11}C]MRB distribution volume

Based on previous modeling studies of [^{11}C]MRB kinetics (Logan et al., 2005; Gallezot et al., 2007), [^{11}C]MRB volume of distribution (V_T) was estimated using the multilinear analysis MA1 (Ichise et al., 2002) and the following equation:

$$C_T(t) = -\frac{V_T}{b}\int_0^t C_p(u)\,du + \frac{1}{b}\int_0^t C_T(u)\,du, \quad t>t^* \qquad (2)$$

where the parameter b is equivalent to the y-intercept in the Logan plot (Logan et al., 1990). When MA1 was applied to the regional time activity curves, t^* was set to 30 min. Parametric images of the V_T of [^{11}C]MRB were also computed using MA1. In these pixel-by-pixel analyses, t^* was set to 10 min.

Quantification of [^{11}C]MRB binding potential without arterial blood sampling

In order to avoid using arterial blood sampling, the ratio of the V_T of [^{11}C]MRB in a target region (or voxel) to that in a reference region, V_T/V_{Ref}, was estimated using MRTM2 (Ichise et al., 2003). MRTM2 is based on the multilinear reference tissue model (MRTM) (Ichise et al., 1996, 2003) and the following equation:

$$C_T(t) = -\frac{1}{b}\frac{V_T}{V_{Ref}}\int_0^t C_{Ref}(u)\,du + \frac{1}{b}\int_0^t C_T(u)\,du + \frac{b'}{b}\frac{V_T}{V_{Ref}}C_{Ref}(t), \quad t>t^* \qquad (3)$$

where the parameter b' is the y-intercept in the Logan plot of the reference region. The parameter b' is also equal to the value of the parameter b, in Eq. (2), for the reference region. Therefore, in theory, the parameter b' should be identical in all voxels or regions for any given scan. However, in MRTM, one value of b' is estimated per ROI or voxel. With MRTM2, only one value of b' is estimated per scan in order to reduce the variability of the other parameter estimates.

MRTM2 is a two-step procedure. In the first step, MRTM was applied to all brain voxels to produce parametric images of BP_{ND}, b and b', as well as a parametric image of the standard error $\sigma_{b'}$ of parameter b' determined from the linear fit. Then a global estimate of b' was computed using the following weighted mean formula over all brain voxels:

$$b'_{MRTM2} = \Sigma\frac{b'}{\sigma^2_{b'}} / \Sigma\frac{1}{\sigma^2_{b'}} \qquad (4)$$

Then, in the second step, MRTM was reapplied to all brain voxels using the aforementioned *b'* value as a fixed parameter, to produce improved parametric images of BP_{ND} and *b*. To compute these MRTM2 parametric images, only the caudate nucleus was used as reference region.

Estimation of ATX IC_{50} and ED_{50}

Three indexes of [^{11}C]MRB binding were compared to highlight the dose-dependent effect of ATX and quantify its IC_{50}: the normalized distribution volume V_T/f_P, and the binding potentials BP_F and BP_{ND} (Innis et al., 2007). V_T/f_P and BP_F values were obtained from the MA1 V_T estimates. BP_{ND} values were obtained either from the MA1 V_T estimates or directly from the MRTM2 analyses. The effect of ATX on these three indexes was quantified using the following equations:

$$\frac{V_T}{f_P} = \frac{V_{ND}}{f_P} + \frac{B_{max}}{K_d}\frac{1}{1+\frac{C_{ATX}}{IC_{50}}} \quad (5)$$

$$BP_F = \frac{V_T - V_{Ref}}{f_P} = \frac{B_{max}}{K_d}\frac{1}{1+\frac{C_{ATX}}{IC_{50}}} \quad (6)$$

$$BP_{ND} = \frac{V_T - V_{Ref}}{V_{Ref}} = \frac{f_{ND}B_{max}}{K_d}\frac{1}{1+\frac{C_{ATX}}{IC_{50}}} \quad (7)$$

where C_{ATX} is the average concentration of ATX measured in the plasma during the PET scan (i.e., the average of the three samples taken 120, 180 and 240 min after the beginning of the ATX infusion), B_{max} is the NET density, K_d is [^{11} C]MRB equilibrium dissociation constant, V_{ND} and V_{Ref} are the non-displaceable distribution volumes in the target tissue and in the reference region, respectively, and f_{ND} and f_P are the free fractions of [^{11} C] MRB in the target tissue (excluding specific binding) and in plasma, respectively. Eq. (5) is a 3-parameter equation (V_{ND}/f_P, B_{max}/K_d and the IC_{50}). Eqs. (6) and (7) are 2-parameter equations (B_{max}/K_d and the IC_{50} for Eq. (6); $f_{ND}B_{max}/K_d$ and the IC_{50} for Eq. (7)), and are based on the assumption that V_{ND} in the target tissue is equal to V_T in the reference region (i.e., V_{ND}= V_{Ref}). Three candidate reference regions were evaluated: putamen, caudate nucleus and occipital cortex. IC_{50} estimates were obtained using each target region by pooling data from all monkeys. For each region, data from all monkeys was pooled, and fitted with one set of parameters, ignoring the effects of the population variability of V_{ND}/f_P, B_{max}/K_d, $f_{ND}B_{max}/K_d$ and IC_{50} in this small sample.

Alternatively, the percentage of occupancy was estimated for each scan using the Lassen plot (Lassen et al., 1995; Cunningham et al., 2010). This method assumes that all the regions included in the analysis have identical non-specific binding (i.e. V_{ND}/f_P) and ATX occupancy level. Therefore, regions which were estimated to have different V_{ND}/f_P values were excluded (see results). In the Lassen plot, the reduction of V_T/f_P between a baseline scan and a post-drug scan is plotted against the corresponding V_T/f_P estimates at baseline. Then, ATX occupancy was estimated for each scan as the slope of the regression line. Then, ATX IC_{50} was estimated by fitting the curve representing ATX occupancy versus the ATX plasma concentration C_{ATX} using the following equation:

$$\text{occupancy}=\frac{C_{ATX}}{C_{ATX}+IC_{50}} \quad (8)$$

Finally, the IC_{50} estimates (ng/mL plasma) were converted to ED_{50} estimates (mg/kg/h) using the linear correlation between the measured ATX plasma levels and the infusion rates.

Data weights, parameter estimation and statistical analyses

Parameters V_T (for MA1) and BP_{ND} (for MRTM2) were estimated using multilinear weighted least squares, with weights based on the noise-equivalent counts in each frame. For the estimation of ATX IC_{50}, nonlinear parameter estimation was performed using a Marquardt–Levenberg algorithm (Marquardt, 1963) and custom software for IDL 6.2 (ITT Visual Information Solutions, Boulder, CO, USA). Standard errors on the fitted parameters were estimated using the theoretical covariance matrix (Beck and Arnold, 1977, chapter 7.7.1).

Standard errors on the plasma free fraction (σ_{fP}) were estimated using the standard deviation of the triplicate measurements of plasma (σ_C***plasma) and ultrafiltrate (σ_C***ultrafiltrate) samples, and the error propagation equation. Similarly, the standard error on the normalized distribution volumes V_T/f_P were also computed using the error propagation equation.

F tests were used to determine whether the parameters IC_{50} and V_{ND}/f_P could be shared across NET-rich regions. Similarly, *F* tests were used to determine whether the parameter B_{max}/K_d could be set to zero in the candidate reference regions, or if the value of V_{ND}/f_P estimated from a reference region was compatible with data from the high-binding regions.

Results

ATX plasma levels

For all monkeys and all ATX doses, ATX plasma levels could be considered stable 120 min after the beginning of the first infusion (i.e. throughout the PET scan), and ranged between 12 ng/mL and 132 ng/mL (Fig. 2A–C). The percent change per hour of ATX plasma level during the PET scan was −1±6%/h. Moreover, ATX plasma levels and the infusion rate were well correlated (Fig. 2D). The slope of the regression line was 1.04 kg×h/L (body weight×time/plasma volume) (r^2=0.902, n=7, intercept set to zero).

[^{11}C]MRB input function

The radioactivity concentration in whole blood was always slightly lower than that in plasma. The whole blood to plasma concentration ratio was 0.94±0.13 throughout the scans. The fraction of unmetabolized [^{11}C]MRB in plasma quickly decreased initially and then stabilized (Fig. 3A): it was 42±8% and 25±4% at 20 and 90 min post-injection, respectively. Since the last parent fraction measurement was only done at 90 min, the metabolite correction from 90 to 120 min was based on the extrapolation of the fits obtained with Eq. (1) and shown in Fig. 3A. The relative difference between the distribution volumes estimated using 120 min worth of PET data (with extrapolation of the unchanged fraction curve) versus 90 min was +5±6% in the high binding regions and +3±2% in the NET-poor regions.

[^{11}C]MRB plasma free fraction f_P was highly variable from scan to scan, with two main trends (Fig. 3B). First, there was a moderate increase from the first to the second scan of the day (+17%±10%). Also, there was a higher day-to-day variability (−16% and −68% for

monkey #1 and #3, respectively). The relative standard errors on the free fraction f_P measurement were less than 10% for all studies (5% in average) suggesting that these differences were not due to measurement error.

[^{11}C]MRB distribution volumes and normalized distribution volumes

Typical regional time–activity curves at baseline and the corresponding fitted curves obtained with MA1 in one monkey are shown in Fig. 4. [^{11}C]MRB distribution volumes (V_T) estimated using MA1 (t^*=30 min) are listed in Table 1. The relative standard errors on V_T estimates were less than 9% for all studies and ROIs (3% in average). Although the distribution volumes were variable from day to day, especially for monkey #3, V_T values estimated in the candidate reference regions were highly correlated with the plasma free fraction f_P (e.g., in the caudate nucleus V_T=25.2 f_P+0.3, r^2=0.920, n=10). The normalized volumes of distribution values (V_T/f_P) decreased in a dosedependent manner with increased ATX doses for all monkeys in all the NET-rich regions (Fig. 5). This relationship was not clearly detectible when V_T values were used without f_P normalization.

Estimation of ATX IC_{50} in high binding regions

Plots of V_T/f_P values versus the plasma concentration of ATX are displayed in Fig. 6A to C for three NET-rich regions. Using only the normalized distribution values V_T/f_P, ATX IC_{50} values were estimated in four NET-rich regions, without using a reference region. It is possible to fit the data from these four regions with a global IC_{50} value and a global V_{ND}/f_P value without significantly increasing the residual sum of squares ($F_{6,28}$=0.17, p=0.98). The global IC_{50} estimate was 32±13 ng/mL (rSE =39%) and the global V_{ND}/f_P estimate was 19±4 mL/cm^3 (rSE=22%). The corresponding fitted curves are displayed in Fig. 6A to C. This corresponds to a global effective dose (ED_{50}) of 0.031 mg/kg/h using the relationship between plasma levels and the maintenance infusion shown in Fig. 2D (i.e., C_{ATX}=MIR_{ATX}×1.042 kg×h/L). Based on this global IC_{50} estimate and the measured ATX plasma concentration, the percentage of occupancy of NET by ATX achieved in this study was estimated to range from 27% (at 12 ng/mL) to 80% (at 132 ng/mL).

Using the global V_{ND}/f_P estimate, BP_{ND} was computed as V_T/f_P at baseline divided by V_{ND}/f_P, minus one, and was estimated to range from 1.4±0.2 in the midbrain to 1.8±0.3 in the thalamus (n=3). These BP_{ND} values being very sensitive to the estimation of V_{ND}/f_P, a more conservative approach was also used to estimate a lower bound for BP_{ND}: BP_{ND} was computed was V_T/f_P at baseline divided by V_T/f_P at the highest doses of ATX, minus one. That is, a 100% occupancy was assumed at the highest doses of ATX in this second approach. With this method BP_{ND} was estimated to range from 1.0±0.04 in the midbrain to 1.2±0.5 in the thalamus (n=2, since one monkey did not have a high-dose scan).

Evaluation of candidate reference regions

The relative standard error on the aforementioned IC_{50} estimate was large (39%) due to the need to estimate the extra parameter V_{ND}/f_P. To try to reduce that uncertainty of the IC_{50} estimate, and also to potentially avoid arterial blood sampling, the use of a reference region was investigated. The normalized distribution volume values V_T/f_P at baseline (n=3) were very similar for all three candidate reference regions, i.e., 30±2 mL/cm^3, 30±2 mL/cm^3 and 28±3 mL/cm^3 for putamen, occipital cortex, and caudate nucleus, respectively. These baseline V_T/f_P values were higher than the V_T/f_P values after blockade by the highest dose of ATX in NET-rich regions: V_T/f_P was estimated to be 24±3, 26±3, 23±1 and 24±1 in the anterior cingulate cortex, thalamus, midbrain and brainstem, respectively, after blockade by the highest dose of ATX (n=2). These baseline V_T/f_P values were also higher than the previously estimated value of V_{ND}/f_P in the four high-binding regions (i.e., 19±4 mL/cm^3). These differences could be due to differences in V_{ND} between the candidate reference

regions and the high-binding regions, or due to the presence of specific binding in the candidate reference regions.

To test for the presence of specific binding, the curves of V_T/f_P values versus the plasma concentration of ATX in the three reference regions were fitted using Eq. (5), with the IC_{50} parameter fixed to the global value estimated in high-binding regions (i.e., 32 ng/mL). The data was fitted twice, with or without the assumption that B_{max}/K_d can be fixed to zero (Fig. 6D to F), and the two fits were compared using the F test. In the occipital cortex, assuming that B_{max}/K_d is equal to zero produced a significantly worse fit ($F_{1,8}$=8.4, p<0.02). B_{max}/K_d was estimated to be 10±4 mL/cm^3 and V_{ND}/f_P was estimated to be 20±3 mL/cm^3. Thus, a significant specific binding was detected in occipital cortex; this region was thus excluded from the list of candidate reference regions. In the putamen, assuming that B_{max}/K_d is equal to zero did not produce a significantly worse fit ($F_{1,8}$=0.07, p=0.8). V_{ND}/f_P was then estimated to be 30±1 mL/cm^3. In the caudate, there was a trend-level, but not significant, difference between the two fits ($F_{1,8}$=3.0, p=0.12). With the two-parameter fit, B_{max}/K_d was estimated to be 6±4 mL/cm^3 and V_{ND}/f_P was estimated to be 23±2 mL/cm^3. With the one-parameter fit, V_{ND}/f_P was estimated to be 26±1 mL/cm^3.

To test whether the estimate of V_{ND}/f_P from the putamen (or caudate) is significantly different from the estimate of V_{ND}/f_P from the high-binding regions, the high binding region curves were fitted twice, with or without fixing V_{ND}/f_P to the value estimated in the putamen (or caudate), and the two fits were compared using the F test. Using the V_{ND}/f_P value estimated in the putamen (i.e., 30 mL/cm^3) as a fixed parameter to fit the high-binding region data lead to significantly worse fits ($F_{1,34}$=17.6, p<0.001). Similarly, using the V_{ND}/f_P value estimated in the caudate (i.e., 26 mL/cm^3) as a fixed parameter to fit the high-binding region data lead to significantly worse fits ($F_{1,34}$=6.0, p<0.02). Thus, putamen and caudate are also not perfectly valid reference regions.

Estimation of the bias on IC_{50} estimates when using caudate or putamen as the reference region

Using the caudate as the reference region and the binding potential BP_{ND} (deduced from MA1 V_T estimates), ATX IC_{50} was estimated to be 21±4 ng/mL (rSE=18%), which is 36% lower than the IC_{50} estimate obtained without using a reference region. Similarly, ATX IC_{50} was estimated to be 19±3 ng/mL (rSE=16%) when using BP_F (bias=−39%). Using the putamen as the reference region and either BP_{ND} or BP_F, ATX IC_{50} was estimated to be 9±2 ng/mL (rSE=28%), which is 72% lower than the estimate without using a reference region. Thus, the IC_{50} estimate was both more biased and less precise when using the putamen rather than the caudate nucleus. Additionally, the IC_{50} estimates obtained using caudate-based BP_{ND} or BP_F values are not significantly lower than the IC_{50} estimate obtained using V_T/f_P ($F_{1,34}$<2.3, p>0.14), but the IC_{50} estimates obtained using putamen-based BP_{ND} or BP_F values are significantly lower ($F_{1,34}$=12.6, p<0.002).

In order to avoid arterial blood sampling, [^{11}C]MRB binding potentials were also estimated directly using MRTM2 and the caudate nucleus as a reference region. The estimates of BP_{ND} obtained with MRTM2 and MA1 were highly correlated (y =0.993 x+ 0.021, r^2=0.949, n=70, where x and y represent MA1 and MRTM2 regional BP_{ND} estimates, respectively). MRTM2 BP_{ND} parametric images are visually almost identical to MA1 BP_{ND} images, except for a few artifacts in the images from scans following administration of the highest doses of ATX (data not shown). Consequently, the IC_{50} estimate obtained using MRTM2 BP_{ND} estimates (21±3 ng/mL) was very similar to the one obtained using MA1 BP_{ND} estimates (21±4 ng/mL).

Improving IC_{50} estimates by using occipital as a low binding region

Another approach was tested to reduce the standard error on the IC_{50} estimate: fitting the four high binding regions together with the occipital cortex since both V_{ND}/f_P and the IC_{50} seemed similar in these five regions, using Eq. (5). The relative standard error on V_{ND}/f_P and IC_{50} estimates could be slightly reduced to 15% and 31% (from 22% and 39%, respectively, without including the occipital in the analysis) with negligible changes in the estimates themselves: V_{ND}/f_P and IC_{50} estimates are then 19± 3 mL/cm^3 and 31±10 ng/mL (from 19±4 mL/cm^3 and 32±13 ng/mL, respectively). B_{max}/K_d was estimated to 11±4 in the occipital cortex.

Estimating ATX IC_{50} using the Lassen plot

Lassen plots obtained for the three animals are shown in Fig. 7A–C. The four high binding regions and the occipital were included in the analysis, since the previous analyses showed that V_{ND}/f_P and the IC_{50} were not significantly different in these regions. ATX occupancy estimates were 31±10%, 56±7% and 86±13% for the low-, medium- and high-dose scans for monkey 1, 65±18% for monkey 2, and 39±14%, 63±7% and 82±6% for the low-, medium- and high-dose scans for monkey 3. The relationship between these ATX occupancy estimates and the measured concentration of ATX in plasma is shown in Fig. 7D. ATX IC_{50} was estimated to be 28±7 ng/mL with this method. This IC_{50} value is in excellent agreement with the value obtained above using the nonlinear fit.

Discussion

In this study, we demonstrated that [^{11}C]MRB is a suitable ligand for determination of NET occupancy. We found that [^{11}C]MRB binding can be inhibited in a dose-dependent manner by infusion of ATX. An important methodological consideration was the day-to-day variability of [^{11}C]MRB V_T estimates in anesthetized non-human primate, which can be explained by variations of [^{11}C]MRB plasma free fraction. Thus V_T/f_P is a better index to quantify [^{11}C]MRB *in vivo* binding than V_T. Finally, the suitability of three putative reference regions was investigated. None of them was found to be an ideal reference region, the caudate being the region introducing the least bias in IC_{50} estimates based on BP_{ND} calculations.

Variability of V_T estimates and plasma free fraction f_P

The substantial variability in the V_T estimates for [^{11}C]MRB from scan to scan in anesthetized baboons was previously reported (Logan et al., 2005). Consequently, the normalization of the volumes of distribution estimates by some reference region values was found to be critical, even though no ideal reference region could be identified. In this study, high variations of the V_T estimates were also observed. As a result, without correction by f_P, no dose-dependent reduction of V_T estimates could be consistently observed. However, the V_T estimates in NET-poor regions were highly correlated with the estimates of the plasma free fraction f_P. This result is consistent with the interpretation that a higher plasma free fraction will lead to higher brain uptake and higher values of V_T as well as the non-specific distribution volume V_{ND}, specifically $V_{ND}=f_P/f_{ND}$ (Innis et al., 2007; Eq. (19)). Moreover, the normalized distribution volumes (V_T/f_P) decreased in a dose-dependent manner with increased ATX doses in the NET-rich regions, and were almost stable or slightly decreasing in the NET-poor regions. Thus, the normalized volume of distribution V_T/f_P appears to be a suitable index of [^{11}C]MRB binding for occupancy studies. It is also worth noting that the range of the plasma free fraction f_P values observed in this study (8% to 31%), is favorable as it can be accurately measured for each study.

Using the estimate of V_{ND}/f_P in NET-rich regions (19 mL/cm^3), [^{11}C] MRB tissue free fraction f_{ND} is on the order of 5% (since $f_{ND}=f_P/V_{ND}$). In theory, BP_{ND} should be equal to $f_{ND}\ B_{max}/K_d$. Therefore, using *in vitro* estimates of MRB dissociation constant K_d (2.5 nM) (Melloni et al., 1984) and of the density of the norepinephrine transporters in the thalamus of rhesus monkeys (23–72 nM) (Smith et al., 2006), and the present estimate of f_{ND}, then an expected value of the binding potential BP_{ND} in the thalamus can be computed as 0.46–1.44, in good agreement with the present measured values (1.8±0.3 based on the V_{ND}/f_P estimates from the fits with Eq. (5); 1.2±0.5 based on V_T/f_P estimates from the high-dose scans).

The cause of the variations of the plasma free fraction f_P across experiments in these anesthetized animals could not be explained. No correlations were found between the estimates of the plasma free fraction f_P and physiological recordings (pCO_2, heart rate, respiration rate, level of isoflurane) measured during the anesthesia (data not shown). Interestingly, this f_P variation was not observed in humans (Hannestad et al., 2010).

Estimation of ATX IC_{50} for NET

Based on our PET studies, the preferred method to estimate the IC_{50} of ATX with [^{11}C]MRB was to fit the V_T/f_P values obtained for each scan with Eq. (5), using the four high binding regions and the occipital cortex. Since ATX IC_{50} and [^{11}C]MRB V_{ND}/f_P were not found to be statistically different across these regions, this method is very similar to the Lassen plot method (Lassen et al. 1995; Cunningham et al., 2010), which assumes that these two variables have identical values in all regions. Consequently, the estimates were very similar (31 vs. 28 ng/mL plasma). The differences between the method used in this study and the Lassen plot method lies in the nature of the estimators (nonlinear versus linear fit; uncorrelated versus correlated variables used for the x- and y-axes), and some hypotheses used when estimating V_{ND}/f_P (one V_{ND}/f_P value estimated for all scans and monkeys using Eq. (5), versus seven V_{ND}/f_P values estimated from the Lassen plots).

The IC_{50} of ATX for norepinephrine transporters estimated in this study, i.e. 31 ng/mL plasma or 122 nM (ATX molecular weight=255 g/ mol), is compatible with results from previous *in vitro* studies. Using similar hypotheses as for a radiotracer, the IC_{50} of a drug *in vivo* can be linked to its *in vitro* affinity (K_d) and its plasma free fraction (f_P), by the equation $IC_{50}=K_d/f_P$. ATX *in vitro* K_d was estimated to be 3.4 nM in rats (Wong et al., 1982) and 2–5 nM in humans (Tatsumi et al., 1997; Bymaster et al., 2002). Plasma free fraction of ATX was estimated to be 11–13% in rats (Mattiuz et al., 2003; Kielbasa et al., 2009), 3% in dogs (Mattiuz et al., 2003) and 1.3% in humans (Sauer et al., 2003). The IC_{50} predicted from these K_d and f_P values would be between 15 nM and 385 nM (i.e., 4–98 ng/mL). Despite the approximations in these calculated values, especially due to the species differences, the order of magnitude matches with the present IC_{50} estimate.

The present IC_{50} estimate is also compatible with a previous [^{18}F] F-MeNER-D2 study in which ATX IC_{50} was estimated to 16 ng/mL (Takano et al., 2009a). Moreover, the IC_{50} estimated using MRTM2 and caudate as a reference region, as in that [^{18}F]F-MeNER-D2 study, is even closer (21 ng/mL).

The present estimate of the IC_{50} of ATX, 31 ng/mL plasma, is much lower than the plasma levels which were measured during the previous study of ATX and [^{11}C]MRB in humans (Logan et al., 2007): there, the plasma levels of ATX were 116, 206, and 421 ng/mL for the three clinically relevant doses of 25, 50 and 100 mg oral ATX, respectively. Based on the present IC_{50} estimate, the lack of an obvious dose-dependent effect in that study was indeed due to the fact that those three clinically relevant doses all reached saturation with over 78–93% occupancy; i.e., the plateau portion of the corresponding dose-occupancy curve. This extrapolation assumes comparable free fraction of ATX in humans and non-human primates.

Use of a reference region with [^{11}C]MRB in occupancy studies

Norepinephrine transporters are distributed throughout the brain, with relatively low contrast between transporter-poor and transporter-rich regions (locus coeruleus excluded). In rhesus monkeys, the lowest densities measured by autoradiography (Smith et al., 2006) were detected in putamen and caudate: in these two regions, the density of NET is about 5 fmol/mg of wet brain tissue, which represents between 7% and 22% of the densities measured in the various sub-nuclei of the thalamus in the same study. In the present study, no significant level of specific binding was detected in the caudate (p=0.12) and putamen (p=0.8). However, the non-displaceable binding appeared higher in the caudate (V_{ND}/f_P=26 mL/cm^3) and putamen (V_{ND}/f_P=30 mL/cm^3) than in the NET-rich region (V_{ND}/f_P=19 mL/cm^3). This lead to an underestimation of BP_{ND} or BP_F values, and subsequently to an underestimation of the IC_{50} of ATX (by 36–39% with caudate and 72% with putamen). This non-uniform level of non-specific binding throughout the brain has been reported for [^{11}C]MRB in baboons (Logan et al., 2005) and humans (Logan et al., 2007). This issue is also not specific to [^{11}C]MRB: a higher level of non-specific binding in the putamen was also reported for previous radiotracers developed to target norepinephrine transporters (such as [^{11}C]oxaprotiline and [^{11}C] lortalamine) (Ding et al., 2005). It is also worth noting that such small between-region difference in non-specific binding may exist for many PET tracers. However, the effect of such variation is more pronounced, and therefore more easily detectible, for tracers with relatively low BP_{ND} values. An alternative possibility is that the apparent higher non-specific binding in the basal ganglia is in fact due to a small amount of specific binding, but that the variability of the V_T/f_P estimates was too high, or the number of experiment too low, to detect a statistically significant blockade in these NET-poor regions. Finally, one limitation of the present study is that V_{ND}/f_P was estimated based on fits of the occupancy data. Studies at higher occupancy levels than in this study (i.e., >90%) would be useful to confirm these findings.

The occipital cortex was investigated since in one *in vitro* autoradiography study in humans using [^{18}F]F-MeNER-D$_2$, the lowest concentration of NET was found in the occipital cortex (Schou et al., 2005). However, a significant reduction of [^{11}C]MRB V_T/f_P after ATX infusion was observed in the present study. Conversely, the level of non-specific binding in the occipital cortex seems to be similar to the one in the main regions of interest. The difference between this study and the aforementioned *in vitro* autoradiography study could be due to difference of species, as well as differences in the delineation of the region of interest. In fact, the suitability of the occipital cortex as a reference region in humans for [^{11}C]MRB has been assessed by blocking studies in humans: [^{11}C]MRB average V_T in the occipital cortex was reduced by 10% after the administration of 100 mg of ATX (Logan et al., 2007), and a reduction of 9±17% for V_T and 5±15% for V_T/f_P was observed after the administration of 40 mg of methylphenidate (n=9;Hannestad et al., 2010). Therefore, the fraction of displaceable binding in the occipital cortex for [^{11}C]MRB may be higher in rhesus monkeys than in humans.

Since the normalized distribution volume (V_T/f_P) can be measured accurately and shown to reduce in a dose-dependent manner, it is not necessary to use a reference region for occupancy studies. However, only relying on V_T/f_P to quantify [^{11}C]MRB binding in an occupancy study would lead to a potentially larger uncertainty in the estimated IC_{50}, since there is one additional parameter to be estimated (i.e., the normalized non-displaceable volume of distribution V_{ND}/f_P). To improve the estimation of this extra parameter, an additional scan using a very high dose of the blocking drug (targeting >90% occupancy) would be required. However, using such a high blocking dose of the drug may not be feasible due to the potential toxicity of the drug. Alternatively, using a “reference” region to avoid estimating V_{ND}/f_P could lead to some bias in the estimated IC_{50}, when the so called “reference” region contains some specific binding, or when that region’s non-specific

binding is not representative of other regions of interest. This presents a classical trade-off between maximizing precision (i.e., reducing the standard error of the IC_{50} estimate) and accuracy (i.e., reducing the bias in that IC_{50} estimate). In this study, the caudate nucleus was the "reference" region, which leads to the least bias (36–39%). This bias is not significant as compared to the "gold standard" IC_{50} estimate obtained using only V_T/f_P values. Moreover, similar results were obtained while using the binding potentials BP_F and BP_{ND}. The latter could be estimated without arterial blood sampling by using MRTM2 and provided equivalent results to those obtained with the arterial data, i.e., without introducing further bias.

Interestingly, this issue of selecting a reference region seems to be less troublesome in humans since all three NET-poor regions (caudate, putamen and occipital) were considered as reasonable reference regions based on the results of our occupancy study of methylphenidate (Hannestad et al., 2010). Thus, using MRTM2 with a reference region to quantify [^{11}C]MRB binding without arterial sampling for occupancy studies is feasible in non-human primates and adequate in humans.

Visualization of the locus coeruleus

The region with the highest density of NET, the locus coeruleus, is very small (~10 mm^3 in humans) (Hoogendijk et al., 1995), and thus challenging to quantify accurately with PET, even with the HRRT and the MOLAR algorithm. [^{11}C]MRB binding in the locus coeruleus might still produce a visible signal in rhesus monkeys, but unambiguously identifying the locus coeruleus is not simple: it is not visible on standard T1-weighted MR images, and there are other NET-rich nuclei in the brainstem where the signal may be higher (due to lower partial volume effect) or whose signal may overlap the locus coeruleus signal (due to limited resolution). Noise in the parametric images may also be an issue. Therefore, we limited our quantification to a more global brainstem region.

Comparison of [^{11}C]MRB and [^{18}F]MeNER-D$_2$ for preclinical occupancy studies in rhesus monkeys

In rhesus monkeys, [^{11}C]MRB binding potentials are higher than those of [^{18}F]MeNER-D$_2$: for example in the thalamus, [^{11}C]MRB BP_{ND} was 1.8±0.3, while [^{18}F]MeNER-D$_2$ BP_{ND} was 0.26±0.06 (Seneca et al., 2006) or 0.7±0.1 (Takano et al., 2009a,b). Interestingly, BP_{ND} values for [^{11}C]MRB and [^{18}F]MeNER-D$_2$ were found to be similar in humans (Logan et al., 2007; Ding et al., 2010; Arakawa et al., 2008).

The biggest drawback for [^{18}F]MeNER-D$_2$ is its *in vivo* defluorination which leads to a high uptake of radioactivity in the skull. Though some regions of interest are away from the skull (thalamus, midbrain and brainstem), some part of the cortex, such as the supplemental motor area (Logan et al., 2007), have high concentration of NET and may be potentially useful drug targets. The continuously increasing radioactivity in the skull resulting from in vivo defluorination of [^{18}F]MeNER-D$_2$ during the entire scanning time produces great challenges to accurate quantification of NET binding in the brain cortical areas.

Conversely, the brain time–activity curves are noisy in the late frames with [^{11}C]MRB, as noted in a previous report (Schou et al., 2003). However, we found that the relative standard errors on the V_T estimates were only 3±2% (max=9%). Another potential drawback of [^{11}C]MRB is that the results from this study suggest that there is up to ~30% specific binding, or a higher non-specific binding, in the NET-poor regions (caudate, putamen and occipital), which makes it difficult to choose an ideal reference region. This issue seems to be less troublesome in humans since occipital cortex was considered as a reasonable reference region (Hannestad et al., 2010). It is not clear whether an ideal reference region is

available for [^{18}F]F-MeNER-D_2 in rhesus monkeys, since a detailed comparison of binding potentials estimated using arterial blood sampling versus using a reference region was not performed in the two published occupancy studies in rhesus monkey (Seneca et al., 2006; Takano et al., 2009a).

In general, F-18 tracers are considered advantageous due to their longer half-live which usually provides better count levels at the end of the scan, especially for tracers with slow kinetics. However, drug occupancy studies may be executed more efficiently with C-11 tracers. Occupancy studies in humans typically include a measurement of baseline receptor availability and at least two measures of occupancy per subject, measured at appropriate times post-dose. In anesthetized animals, it is common to test a range of doses within the same animal. The short half-life of C-11 permits two of these scans to be performed in the same day on the same subject. This reduces the number of visits needed, and scans on one day also tend to have less variability, allowing the study to be accomplished with a smaller sample size of subjects. Furthermore, when proper quantification with arterial input function is needed in humans, thus, the C-11 design is clearly more practical since it can be accomplished in a 2-day study design, with the use of arterial lines in one arm per day.

Conclusions

This study demonstrates that [^{11}C]MRB binding *in vivo* can be inhibited in a dose-dependent manner by ATX, and the variability of [^{11}C]MRB distribution volumes in anesthetized monkeys could be explained and corrected by the underlying variability of the plasma free fraction of [^{11}C]MRB. Therefore [^{11}C]MRB is suitable for drug occupancy studies of norepinephrine transporters. Since no ideal reference region could be identified, the gold standard method to estimate the IC_{50} of drugs with [^{11}C]MRB would be the Lassen plot method or the nonlinear fits described in this study. However, it is feasible to use MRTM2 with a reference region to quantify [^{11}C]MRB binding without arterial sampling for occupancy studies. Among the candidate reference regions evaluated, the caudate nucleus has the most desirable properties in rhesus monkeys.

The ED_{50} of ATX was estimated to be 0.028 mg/kg/h (or 0.13 mg/kg), which is much lower than the therapeutic dose of ATX in ADHD (1.0–1.5 mg/kg). This explains why no obvious dose-dependent effect could be seen in the previous PET occupancy study of ATX in humans (Logan et al., 2007).

Acknowledgments

The authors thank the staff of the Yale University PET Center for their technical expertise and support. Funding for this study was provided by the Yale Pfizer Bioimaging Alliance. This publication was also made possible by CTSA Grant Number UL1RR024139 from the National Center for Research Resources (NCRR), a component of the National Institutes of Health (NIH), and NIH roadmap for Medical Research. Its contents are solely the responsibility of the authors and do not necessarily represent the official view of NCRR or NIH.

References

Arakawa R, Okumura M, Ito H, Seki C, Takahashi H, Takano H, Nakao R, Suzuki K, Okubo Y, Halldin C, Suhara T. Quantitative analysis of norepinephrine transporter in the human brain using PET with (S, S)-18F-FMeNER-D2. J. Nucl. Med. 2008; 49:1270–1276. [PubMed: 18632811]

Barker, EL.; Blakely, RD. Norepinephrine and serotonin transporters: molecular targets of antidepressant drugs. In: Bloom, FE.; Kupfer, DJ., editors. Psychopharmacology: the fourth generation of progress. Raven Press; New York, NY: 1995. p. 321-334.

Beck, J.; Arnold, K. Parameter estimation in engineering and science. Wiley; New York, NY: 1977.

Bymaster FP, Katner JS, Nelson DL, Hemrick-Luecke SK, Threlkeld PG, Heiligenstein JH, Morin SM, Gehlert DR, Perry KW. Atomoxetine increases extracellular levels of norepinephrine and dopamine in prefrontal cortex of rat: A potential mechanism for efficacy in attention deficit/hyperactivity disorder. Neuropsychopharmacology. 2002; 27:699–711. [PubMed: 12431845]

Carson RE, Barker WC, Liow J, Johnson CA. Design of a motion-compensation OSEM list-mode algorithm for resolution-recovery reconstruction for the HRRT. IEEE Nucl. Sci. Symp. Conf. Rec. 2003; 5:3281–3285.

Cunningham VJ, Rabiner E, Slifstein M, Laruelle M, Gunn RN. Measuring drug occupancy in the absence of a reference region: the Lassen plot re-visited. J. Cereb. Blood Flow Metab. 2010; 30:46–50. [PubMed: 19738632]

Ding YS, Lin KS, Garza V, Carter P, Alexoff D, Logan J, Shea C, Xu Y, King P. Evaluation of a new norepinephrine transporter PET ligand in baboons, both in brain and peripheral organs. Synapse. 2003; 50:345–352. [PubMed: 14556239]

Ding YS, Lin KS, Logan J, Benveniste H, Carter P. Comparative evaluation of positron emission tomography radiotracers for imaging the norepinephrine transporter: (S, S) and (R, R) enantiomers of reboxetine analogs ([11C]methylreboxetine, 3-Cl-[11C]methylreboxetine and [18F]fluororeboxetine), (R)-[11C]nisoxetine, [11C] oxaprotiline and [11C]lortalamine. J. Neurochem. 2005; 94:337–351. [PubMed: 15998285]

Ding YS, Lin KS, Logan J. PET imaging of norepinephrine transporters. Curr. Pharm. Des. 2006; 12:3831–3845. [PubMed: 17073682]

Ding YS, Singhal T, Planeta-Wilson B, Gallezot JD, Nabulsi N, Labaree D, Ropchan J, Henry S, Williams W, Carson RE, Neumeister A, Malison RT. PET imaging of the effects of age and cocaine on the norepinephrine transporter in the human brain using (S,S)-[(11)C]O-methylreboxetine and HRRT. Synapse. 2010; 64:30–38. [PubMed: 19728366]

Gallezot JD, Planeta-Wilson B, Wang GJ, Carson RE, Ding YS. Kinetic modeling of the net radioligand [C-11]MRB in humans: a test-retest study. J. Cereb. Blood Flow Metab. 2007; 27(Suppl 1):23.

Hannestad J, Gallezot J-D, Planeta-Wilson B, Lin S-F, Williams WA, van Dyck CH, Malison RT, Carson RE, Ding YS. Clinically relevant doses of dethylphenidate significantly occupy norepinephrine transporters in humans in vivo. Biol Psychiatry. 2010; 68:854–860. [PubMed: 20691429]

Hoogendijk WJ, Pool CW, Troost D, van Zwieten E, Swaab DF. Image analyser-assisted morphometry of the locus coeruleus in Alzheimer's disease, Parkinson's disease and amyotrophic lateral sclerosis. Brain. 1995; 118:131–143. [PubMed: 7894999]

Ichise M, Ballinger JR, Golan H, Vines D, Luong A, Tsai S, Kung HF. Noninvasive quantification of dopamine D2 receptors with iodine-123-IBF SPECT. J. Nucl. Med. 1996; 37:513–520. [PubMed: 8772658]

Ichise M, Toyama H, Innis RB, Carson RE. Strategies to improve neuroreceptor parameter estimation by linear regression analysis. J. Cereb. Blood Flow Metab. 2002; 22:1271–1281. [PubMed: 12368666]

Ichise M, Liow JS, Lu JQ, Takano A, Model K, Toyama H, Suhara T, Suzuki K, Innis RB, Carson RE. Linearized reference tissue parametric imaging methods: Application to [^{11}C]DASB positron emission tomography studies of the serotonin transporter in human brain. J. Cereb. Blood Flow Metab. 2003; 23:1096–1112. [PubMed: 12973026]

Innis RB, Cunningham VJ, Delforge J, Fujita M, Gjedde A, Gunn RN, Holden J, Houle S, Huang SC, Ichise M, Iida H, Ito H, Kimura Y, Koeppe RA, Knudsen GM, Knuuti J, Lammertsma AA, Laruelle M, Logan J, Maguire RP, Mintun MA, Morris ED, Parsey R, Price JC, Slifstein M, Sossi V, Suhara T, Votaw JR, Wong DF, Carson RE. Consensus nomenclature for in vivo imaging of reversibly binding radioligands. J. Cereb. Blood Flow Metab. 2007; 27:1533–1539. [PubMed: 17519979]

Johnson CA, Thada S, Rodriguez M, Zhao Y, Iano-Fletcher AR, Liow J, Barker WC, Martino RL, Carson RE. Software architecture of the MOLAR-HRRT reconstruction engine. IEEE Nucl. Sci. Symp. Conf. Rec. 2004; 6:3956–3960.

Kaufman MJ, Spealman RD, Madras BK. Distribution of cocaine recognition sites in monkey brain: I. in vitro autoradiography with [3H]CFT. Synapse. 1991; 9:177–187. [PubMed: 1776130]

Kielbasa W, Kalvass JC, Stratford R. Microdialysis evaluation of atomoxetine brain penetration and central nervous system pharmacokinetics in rats. Drug Metab. Dispos. 2009; 37:137–142. [PubMed: 18936112]

Lin KS, Ding YS. Synthesis, enantiomeric resolution, and selective C-11 methylation of a highly selective radioligand for imaging the norepinephrine transporter with positron emission tomography. Chirality. 2004; 16:475–481. [PubMed: 15236345]

Lin KS, Ding YS, Kim SW, Kil KE. Synthesis, enantiomeric resolution, F-18 labeling and biodistribution of reboxetine analogs: promising radioligands for imaging the norepinephrine transporter with Positron Emission Tomography. Nucl. Med. Biol. 2005; 32:415–422. [PubMed: 15878511]

Lassen NA, Bartenstein PA, Lammertsma AA, Prevett MC, Turton DR, Luthra SK, Osman S, Bloomfield PM, Jones T, Patsalos PN. Benzodiazepine receptor quantification in vivo in humans using [11C]flumazenil and PET: application of the steady-state principle. J. Cereb. Blood Flow Metab. 1995; 15:152–165. [PubMed: 7798333]

Logan J, Fowler JS, Volkow ND, Wolf A, Dewey SL, Schlyer D, Macgregor R, Hitzemann, Bendriem, Gatley S, Christman D. Graphical analysis of reversible radioligand binding from time–activity measurements applied to [N-^{11}C -methyl]-(-)-cocaine PET studies in human subjects. J. Cereb. Blood Flow Metab. 1990; 10:740–747. [PubMed: 2384545]

Logan J, Ding YS, Lin KS, Pareto D, Fowler JS, Biegon A. Modeling and analysis of PET studies with norepinephrine transporter ligands: The search for a reference region. Nucl. Med. Biol. 2005; 32:531–542. [PubMed: 15982584]

Logan J, Wang GJ, Telang F, Fowler JS, Alexoff D, Zabroski J, Jayne M, Hubbard B, King P, Carter P, Shea C, Xu Y, Muench L, Schlyer D, Learned-Coughlin S, Cosson V, Volkow ND, Ding YS. Imaging the norepinephrine transporter in humans with (S, S)-[11C]O-methyl reboxetine and PET: Problems and progress. Nucl. Med. Biol. 2007; 34:667–679. [PubMed: 17707807]

Marquardt D. An algorithm for least square estimation of nonlinear parameters. SIAM J. Appl. Math. 1963; 11:431–441.

Mattiuz EL, Ponsler GD, Barbuch RJ, Wood PG, Mullen JH, Shugert RL, Li Q, Wheeler WJ, Kuo F, Conrad PC, Sauer JM. Disposition and metabolic fate of atomoxetine hydrochloride: Pharmacokinetics, metabolism, and excretion in the Fischer 344 rat and beagle dog. Drug Metab. Dispos. 2003; 31:88–97. [PubMed: 12485957]

Melloni PCG, Della Torre A, Bonsignori A, Buonamici M, Pozzi ORS, Rossi AC. Potential antidepressant agents. A-aryloxy-benzyl derivatives of ethanol-amine and morpholine. Eur. J. Med. Chem. 1984; 19:235–242.

Morón JA, Brockington A, Wise RA, Rocha BA, Hope BT. Dopamine uptake through the norepinephrine transporter in brain regions with low levels of the dopamine transporter: Evidence from knock-out mouse lines. J. Neurosci. 2002; 22:389–395. [PubMed: 11784783]

Nabulsi N, Huang Y, Weinzimmer D, Ropchan J, Frost JJ, McCarthy T, Carson RE, Ding YS. High-resolution imaging of brain 5-HT$_{1B}$ receptors in the rhesus monkey using [^{11}C]P943. Nucl. Med. Biol. 2010; 37:205–214. [PubMed: 20152720]

Sauer J, Ponsler GD, Mattiuz EL, Long AJ, Witcher JW, Thomasson HR, Desante KA. Disposition and metabolic fate of atomoxetine hydrochloride: The role of CYP2D6 in human disposition and metabolism. Drug Metab. Dispos. 2003; 31:98–107. [PubMed: 12485958]

Schou M, Halldin C, Sóvágó J, Pike VW, Gulyás B, Mozley PD, Johnson DP, Hall H, Innis RB, Farde L. Specific in vivo binding to the norepinephrine transporter demonstrated with the PET radioligand, (S, S)-[11C]MeNER. Nucl. Med. Biol. 2003; 30:707–714. [PubMed: 14499328]

Schou M, Halldin C, Sóvágó J, Pike VW, Hall H, Gulyás B, Mozley PD, Dobson D, Shchukin E, Innis RB, Farde L. PET evaluation of novel radiofluorinated reboxetine analogs as norepinephrine transporter probes in the monkey brain. Synapse. 2004; 53:57–67. [PubMed: 15170818]

Schou M, Halldin C, Pike VW, Mozley PD, Dobson D, Innis RB, Farde L, Hall H. Post-mortem human brain autoradiography of the norepinephrine transporter using (S, S)-[18F]FMeNER-D2. Eur. Neuropsychopharmacol. 2005; 15:517–520. [PubMed: 16139169]

Seneca N, Gulyás B, Varrone A, Schou M, Airaksinen A, Tauscher J, Vandenhende F, Kielbasa W, Farde L, Innis RB, Halldin C. Atomoxetine occupies the norepinephrine transporter in a dose-

dependent fashion: A PET study in nonhuman primate brain using (S, S)-[18F]FMeNER-D2. Psychopharmacology (Berl). 2006; 188:119–127. [PubMed: 16896954]

Smith HR, Beveridge TJ, Porrino LJ. Distribution of norepinephrine transporters in the non-human primate brain. Neuroscience. 2006; 138:703–714. [PubMed: 16427744]

Spencer TJ, Biederman J, Wilens TE, Faraone SV. Novel treatments for attention-deficit/hyperactivity disorder in children. J. Clin. Psychiatry. 2002; 63(Suppl 12):16–22. [PubMed: 12562057]

Takano A, Gulyás B, Varrone A, Maguire RP, Halldin C. Saturated norepinephrine transporter occupancy by atomoxetine relevant to clinical doses: a rhesus monkey study with (S, S)-[(18)F]FMeNER-D(2). Eur. J. Nucl. Med. 2009a; 36:1308–1314.

Takano A, Gulyás B, Varrone A, Halldin C. Comparative evaluations of norepinephrine transporter radioligands with reference tissue models in rhesus monkeys: (S, S)-[(18)F]FMeNER-D(2) and (S, S)-[(11)C]MeNER. Eur. J. Nucl. Med. 2009b; 36:1892–1895.

Tatsumi M, Groshan K, Blakely RD, Richelson E. Pharmacological profile of antidepressants and related compounds at human monoamine transporters. Eur. J. Pharmacol. 1997; 340:249–258. [PubMed: 9537821]

Wilson AA, Johnson DP, Mozley D, Hussey D, Ginovart N, Nobrega J, Garcia A, Meyer J, Houle S. Synthesis and in vivo evaluation of novel radiotracers for the in vivo imaging of the norepinephrine transporter. Nucl. Med. Biol. 2003; 30:85–92. [PubMed: 12623106]

Wong DT, Threlkeld PG, Best KL, Bymaster FP. A new inhibitor of norepinephrine uptake devoid of affinity for receptors in rat brain. J. Pharmacol. Exp. Ther. 1982; 222:61–65. [PubMed: 6123593]

Zeng Z, Chen TB, Miller PJ, Dean D, Tang YS, Sur C, Williams DL. The serotonin transporter in rhesus monkey brain: Comparison of DASB and citalopram binding sites. Nucl. Med. Biol. 2006; 33:555–563. [PubMed: 16720249]

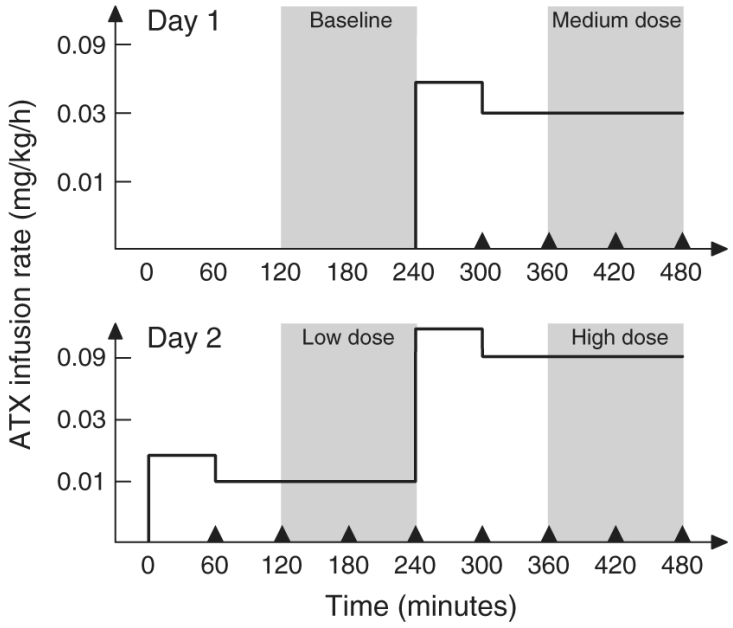

Fig. 1.

Study timelines for the two-day, four-dose studies (Day 1: baseline and medium-dose studies; Day 2: low- and high-dose studies). The solid line represents the ATX infusion rates (i.e., loading rate followed by maintenance rate for each study), as used for monkey #3 (i.e., the maintenance rates were 0.01 mg/kg/h (low dose), 0.03 mg/kg/h (medium dose) and 0.09 mg/kg/h (high dose)). The grey areas highlight the PET scanning times. The black triangles represent the PK sampling times.

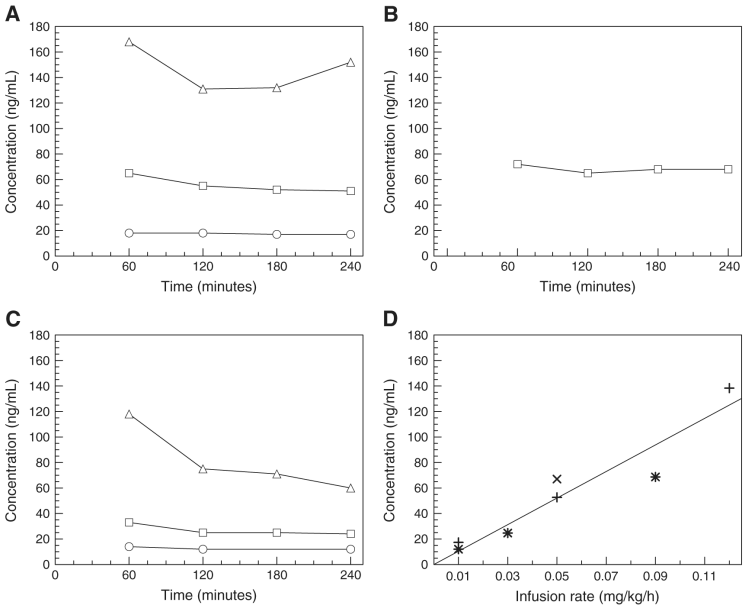

Fig. 2.

(A, B, C) ATX plasma concentration measured for monkeys 1, 2, and 3, respectively, for the low (circle), medium (square) and high (triangle) dose scans. (D) Correlation between the ATX plasma levels and the final infusion rates (infusion II) for monkey 1 (+), 2 (×) and 3 (*), respectively. The regression line was obtained by pooling data from all monkeys (slope=1.04 kg×h/L, r^2=0.902, n=7).

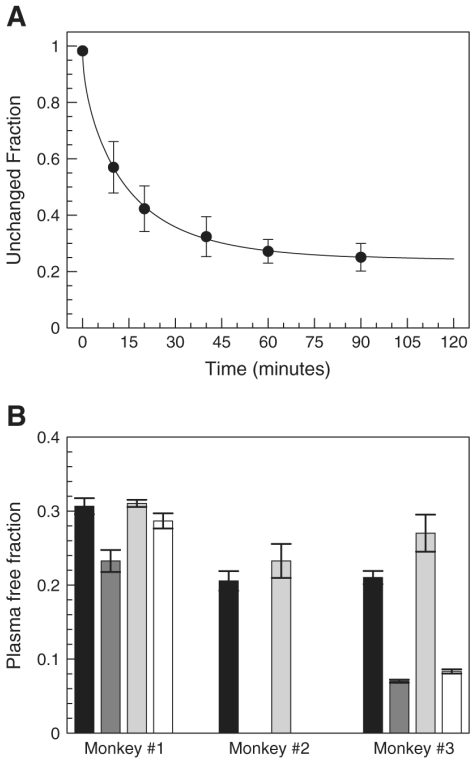

Fig. 3.

(A) Unchanged fraction of [^{11}C]MRB in plasma (average±SD, n=10). The solid line represents the average of the fitted f_H curves used for metabolite correction. (B) [^{11}C]MRB plasma free fraction measured by ultrafiltration for the baseline (black), low (dark grey), medium (light grey) and high (white) ATX dose scans. Errors bars represent the standard errors estimated from the triplicate measurements of plasma and ultrafiltrate activity.

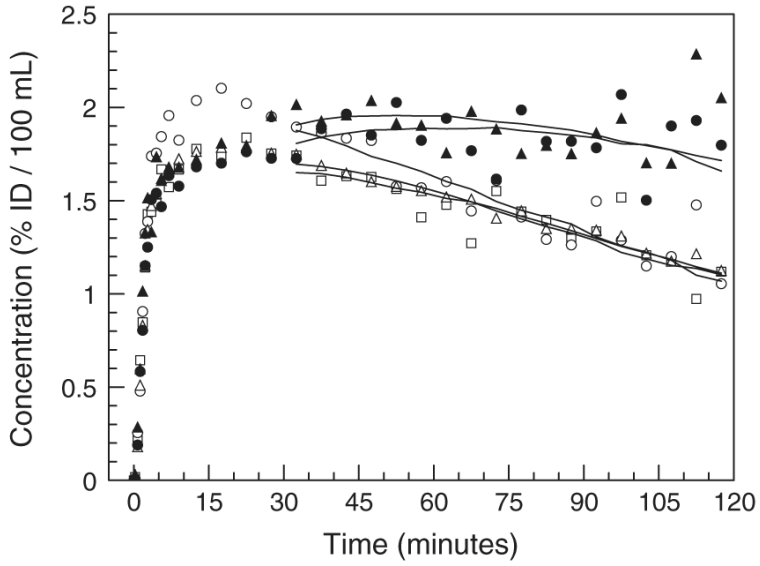

Fig. 4.

Example of regional time activity curves obtained in one monkey (#2) at baseline in the caudate nucleus (open squares), putamen (open circles), occipital cortex (open triangles), anterior cingulate cortex (solid triangles) and thalamus (solid circles). Solid lines correspond to the MA1 fits.

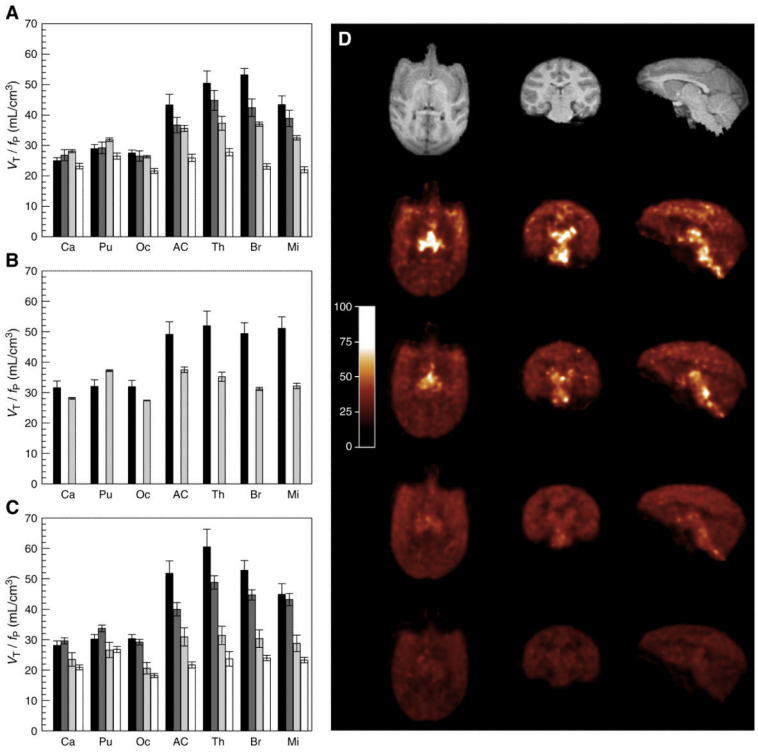

Fig. 5.

Dose-dependent occupancy of ATX in NET-rich regions in three monkeys. (A to C) Normalized volume of distribution (V_T/f_P) computed using MA1 at baseline (black bars) and at the low (dark grey bars), medium (light grey bars) and high (white bars) doses of ATX in the monkeys 1 to 3. The brain regions are: Ca = caudate, Pu = putamen, Oc = occipital cortex, AC = anterior cingulate cortex, Th = thalamus, Br = brainstem, Mi = midbrain. Error bars represent the estimated standard errors. (D) From top to bottom: Anatomic MR image, and parametric images of the normalized volume of distribution (V_T/f_P) at baseline and after blockade with 0.03 mg/kg/h, 0.06 mg/kg/h and 0.12 mg/kg/h of ATX. Images are from monkey #1 and were computed using MA1.

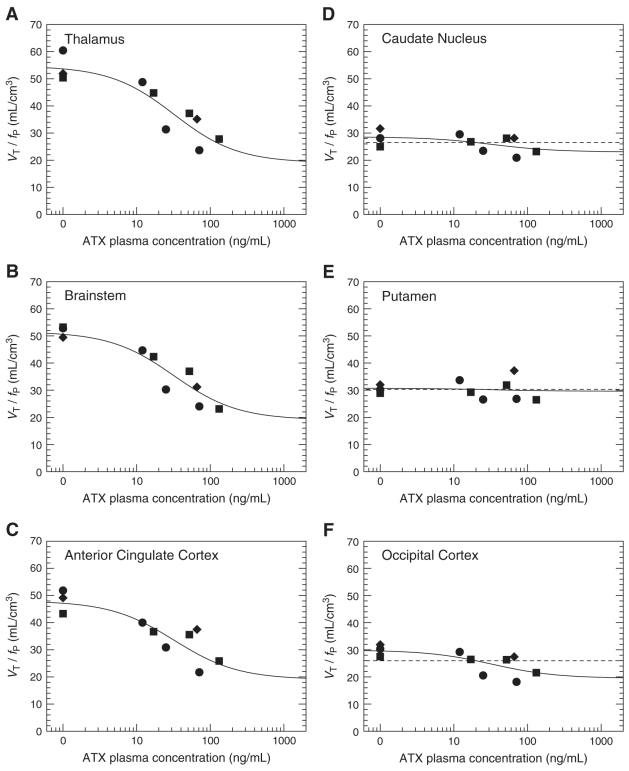

Fig. 6.

The relationship between the normalized distribution volumes (V_T/f_P) and the plasma levels of ATX three NET-rich regions: thalamus (A), brainstem (B) and anterior cingulate cortex (C); and in three candidate reference regions: caudate (D), putamen (E) and occipital cortex (F). Data obtained from monkey 1, 2 and 3 and represented with circles, diamonds and squares, respectively. In subfigures A to C, the solid line represents the fit obtained using Eq. (5) to estimate the ATX IC_{50}. The parameters IC_{50} and V_{ND}/f_P were shared across all NET-rich regions. In subfigures D to F, the two lines represent the fits obtained using Eq. (5), with the IC_{50} set to the value estimated in NET-rich regions (32 ng/mL), and B_{max}/K_d set to zero (dashed line) or fitted (solid line). According to the F test, B_{max}/K_d was significantly different from zero in the occipital only.

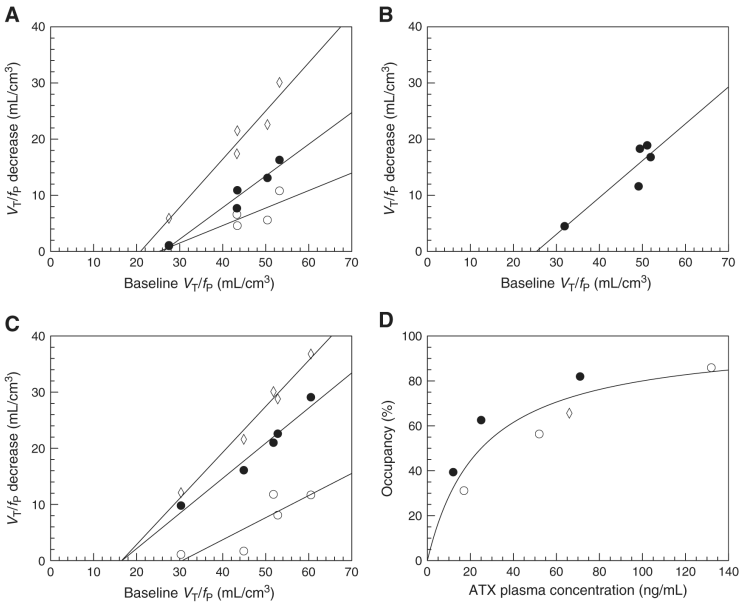

Fig. 7.

Lassen plots obtained for the low (open circles), medium (solid circles) and high (open diamonds) doses for monkeys 1 to 3 are displayed in subfigures A to C. The solid lines represent the regression lines for each set of data. In subfigure D, occupancies estimated as the slope of these regression lines are plotted versus the ATX plasma concentration (monkey 1: open circles; monkey 2: open diamonds, monkey 3: solid circles). Solid line represent the line of best fit obtained with Eq. (8) (pooling data from all monkeys), and corresponding to an IC_{50} estimate of 28±7 ng/mL.

Table 1

[^{11}C]MRB distribution volumes (V_T).

Region	Monkey	Distribution Volume V_T (mL/cm^3)			
		Baseline	ATX low dose	ATX medium dose	ATX high dose
		Day 1	Day 2	Day 1	Day 2
Caudate	#1	7.7	6.2	8.7	6.6
	#2	6.5		6.5	
	#3	5.9	2.1	6.3	1.7
Putamen	#1	8.9	6.8	9.9	7.6
	#2	6.6		8.7	
	#3	6.3	2.4	7.2	2.2
Occipital	#1	8.4	6.2	8.2	6.2
	#2	6.6		6.4	
	#3	6.4	2.0	5.6	1.5
Anterior	#1	13.3	8.5	11.0	7.4
Cingulate	#2	10.1		8.7	
	#3	10.9	2.8	8.3	1.8
Thalamus	#1	15.5	10.4	11.6	8.0
	#2	10.7		8.2	
	#3	12.7	3.4	8.5	2.0
Midbrain	#1	13.3	9.0	10.1	6.3
	#2	10.5		7.5	
	#3	9.4	3.0	7.8	1.9
Brainstem	#1	16.3	9.9	11.5	6.6
	#2	10.2		7.3	
	#3	11.1	3.1	8.2	2.0